

111-08  
61457  
P-32

**NASA Technical Memorandum 102687**

**Trim Drag Reduction Concepts for Horizontal  
Takeoff Single-Stage-To-Orbit Vehicles**

**John D. Shaughnessy and Irene M. Gregory**

(NASA-TM-102687) TRIM DRAG REDUCTION  
CONCEPTS FOR HORIZONTAL TAKEOFF  
SINGLE-STAGE-TO-ORBIT VEHICLES (NASA) 32 p  
CSCL 01C

N92-15076

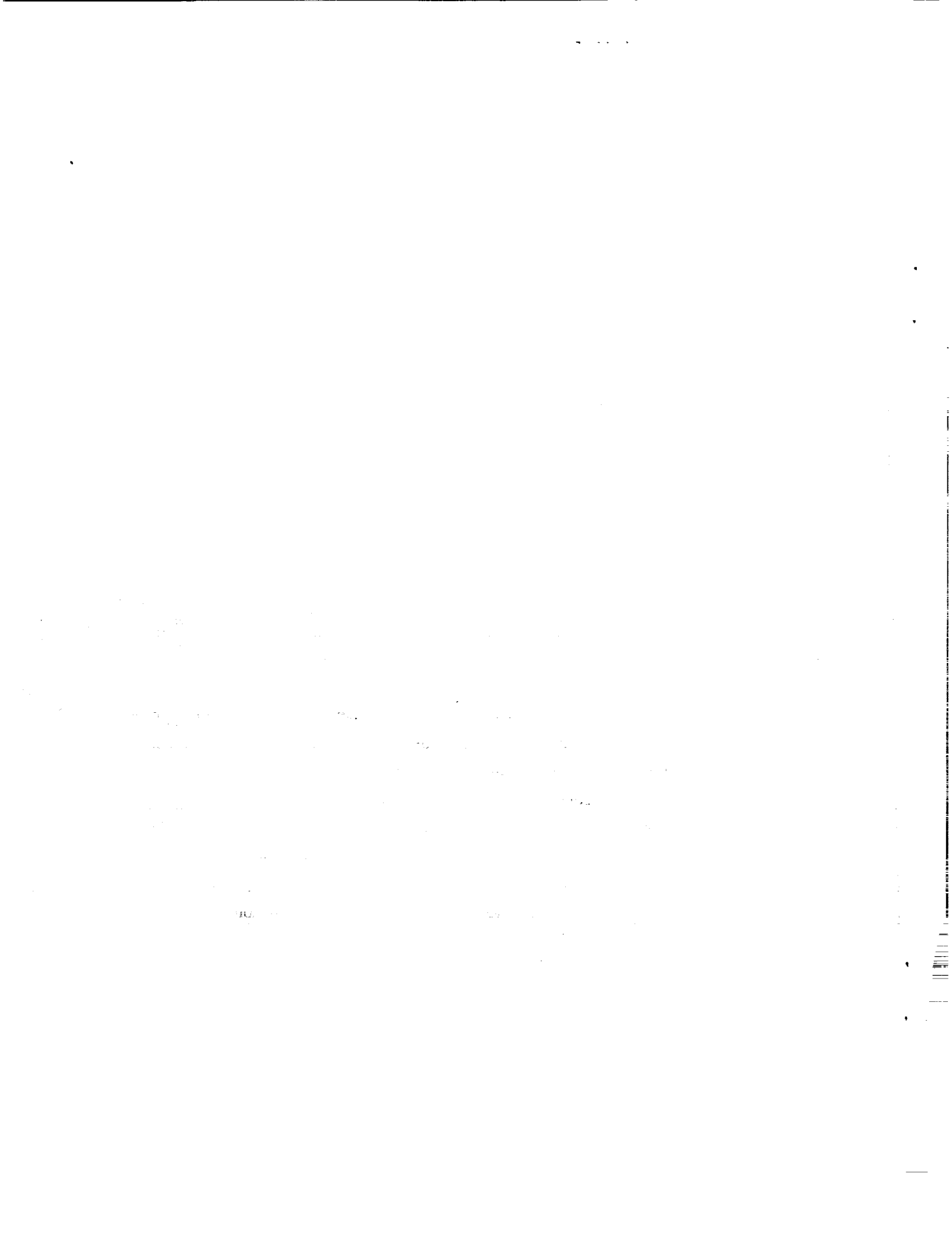
Unclas  
G3/08 0061457

**December 1991**



National Aeronautics and  
Space Administration

Langley Research Center  
Hampton, VA 23665



**Trim Drag Reduction Concepts For Horizontal Takeoff  
Single-Stage-To-Orbit Vehicles**

John D. Shaughnessy and Irene M. Gregory

NASA Langley Research Center

Hampton, Virginia

**SUMMARY**

The results of a study to investigate concepts for minimizing trim drag of horizontal takeoff single-stage-to-orbit (SSTO) vehicles are presented. A generic hypersonic airbreathing conical configuration was used as the subject aircraft. The investigation indicates that extreme forward migration of the aerodynamic center as the vehicle accelerates to orbital velocities causes severe aerodynamic instability and trim moments that must be counteracted. Adequate stability can be provided by active control of elevons and rudder, but use of elevons to produce trim moments results in excessive trim drag and fuel consumption. To alleviate this problem two solution concepts are examined. Active control of the center of gravity (c.g.) location to track the aerodynamic center decreases trim moment requirements, reduces elevon deflections, and leads to significant fuel savings. Active control of the direction of the thrust vector produces required trim moments, reduces elevon deflections, and also results in significant fuel savings. It is concluded that the combination of active flight control to provide stabilization, c.g. position control to minimize trim moment requirements, and thrust vectoring to generate required trim moments has the potential to significantly reduce fuel consumption during ascent to orbit of horizontal takeoff SSTO vehicles.

## SYMBOLS AND ABBREVIATIONS

a.c.	aerodynamic center
APAS	Aerodynamic Preliminary Analysis System
$\alpha$	angle of attack
$\beta$	angle of sideslip
c.g.	center of gravity
$\Delta$ c.g.	change in c.g. position
$\delta_{ELE}$	symmetric elevon deflection
$\delta_{AIL}$	antisymmetric elevon deflection
$\delta_{RUD}$	rudder deflection
$\delta_T$	change in thrust vector angle
F & M	aerodynamic forces and moments
$\phi$	roll angle
$\gamma$	flight path angle
$I_{sp}$	specific impulse
$K_T$	thrust vector gimbal angle gain
m.a.c.	mean aerodynamic chord
M	Mach number
POST	Program to Optimize Simulated Trajectories
p	body axes roll rate
q	body axes pitch rate

$\bar{q}$	dynamic pressure
$r$	body axes yaw rate
SSTO	single-stage-to-orbit
$t$	time
$T$	thrust
T.E.	trailing edge
$\dot{V}$	acceleration along flight path
$W$	weight of vehicle
$x_{cg}$ command	command value of c.g.
$x_{ac}$	longitudinal position of a.c.



## INTRODUCTION

Earth-to-orbit space transportation system concepts have been studied for many years to satisfy anticipated mission needs (refs. 1-4). A key objective of these studies has been to define vehicles that substantially reduce the cost of manned space transportation. These studies have identified concepts using both near-term and more advanced technology. One of the promising concepts using advanced technology is a fully reusable, single stage vehicle with airbreathing propulsion.

This concept is theoretically feasible through the total integration of high specific impulse airbreathing propulsion, lightweight high temperature structural materials, advanced aerodynamic design, and highly integrated flight/propulsion control and guidance systems. A vehicle of this class has never flown and theoretical analyses have shown that the propulsive efficiency of the vehicle will be critical to its success. One way to increase the propulsive efficiency is to reduce the total drag of the vehicle. Drag reduction increases the overall vehicle effective specific impulse.

Beside configuration changes, such as increasing wing sweepback angle and decreasing local surface inclination angles, there are less apparent ways associated with stability and control that can reduce total drag. The aerodynamic center (a.c.) of single-stage-to-orbit (SSTO) class vehicles migrates forward a significant fraction of fuselage length as the vehicle accelerates to orbital speed (refs. 5-10). This migration of the a.c. results in aerodynamic instability and nose-up pitching moments that must be balanced in order to hold the vehicle at required angles of attack (refs. 8, 9). Normally, the balancing trim moment would be generated by deflecting aerodynamic control surfaces; however, even moderate control surface deflections can cause significant trim drag at hypersonic speeds (refs. 11-12). By controlling the center of gravity (c.g.) and causing it to track the a.c., the lift moments and associated trim drag can be reduced, and by controlling the direction of thrust, lift moments can be partially or completely offset, again reducing the trim drag.

The objective of this research is to investigate the potential of two concepts for reducing the trim drag of SSTO vehicles. Control of the c.g. position for reducing trim moment requirements and control of the thrust direction for generating trim moments will be studied. The benefits of these concepts are estimated for the ascent to orbit of a generic SSTO configuration by comparing the fuel consumed from takeoff to orbit with and without each system. A six degrees-of-freedom computer simulation is used to quantify the results.

## ANALYSIS

Study Configuration The vehicle chosen for this study is based on a hypersonic configuration that has been tested experimentally from low subsonic to high hypersonic Mach numbers (refs. 5-7). The full scale vehicle dimensions and gross weight were determined from a vehicle sizing analysis iterated together with point-mass ascent trajectory analyses. This iterative analysis yielded a 200 ft long, 295,000 lb takeoff-weight vehicle. Aerodynamic, propulsion, and mass models for this vehicle, given in reference 15, were developed to allow guidance and flight control studies to be conducted. Appendix A describes the concept of these models.

The planform and side view of the study configuration are shown in figure 1. The vehicle geometric characteristics are given in Table I. The fuselage centerline mounted wing has conventional right and left trailing edge elevons with the hinge line perpendicular to the fuselage centerline. The small canards shown in figure 1 have a 6 percent thick symmetrical 65-A series airfoil and are deployed only at subsonic speeds. In this study, canard incidence is maintained at  $0^\circ$ . The fuselage is modelled as a conical forebody, a cylindrical engine nacelle section, and a cone frustrum afterbody.

Reference Trajectories The reference trajectories basically involved two horizontal takeoff single stage ascents along  $1000 \text{ lb/ft}^2$  and  $2000 \text{ lb/ft}^2$  maximum dynamic pressure paths to an altitude where orbital velocity was obtained followed by a pitch-up maneuver, coasting to a 110 n.m. apogee, and a circularization burn. These trajectories are described in more detail in reference 12, and they are referred to as  $1000 \text{ lb/ft}^2$  and  $2000 \text{ lb/ft}^2$  reference trajectories in this report.

Aerodynamic Center and Center of Gravity Migration The migration of the longitudinal position of the a.c. ( $x_{ac}$ ) and c.g. ( $x_{cg}$ ) as the vehicle accelerates to orbital velocities is shown in figure 2. The quantities  $x_{ac}$  and  $x_{cg}$  are given in terms of percent body length and mean aerodynamic chord as a function of flight Mach number. The APAS program was used to estimate the position of the a.c. as discussed in reference 15. The c.g. position data shown in figure 2 are given in terms of the flight Mach number for the  $2000 \text{ lb/ft}^2$  reference trajectory.

From takeoff to Mach 1 the canard is deployed and the vehicle is aerodynamically unstable longitudinally. When the canard is retracted at Mach 1, the a.c. shifts aft and the vehicle becomes stable. As Mach number increases, the a.c. migrates forward and between Mach 6 and 8 the a.c. moves ahead of the c.g., as shown in figure 2. At this point the vehicle becomes unstable again, and as the velocity increases to orbital values the a.c. moves further forward causing the vehicle to become more unstable longitudinally (and directionally).

The forward migration of the a.c. relative to the c.g. exceeds 35 percent of the m.a.c. and 15 percent of fuselage length. This forward shift of the a.c. with increasing Mach number is characteristic of hypersonic vehicles (refs. 5-10). In addition to the instability problem, the forward travel of the a.c. causes an increasingly large nose-up pitching moment that must be balanced or trimmed in order to hold the vehicle at the desired angle of attack.

Elevon and Vehicle Drag The standard method to counteract the nose-up pitching moment caused by the forward travel of the a.c. would be to deflect the elevons trailing edge down to generate the required nose-down trim moment. The problem with this method is, at hypersonic speeds, even small trailing edge down deflections of elevons cause an unacceptable increase in drag.

To illustrate this elevon trim drag problem, consider a 20° down deflection. The variation of the incremental drag coefficient with Mach number, with and without trailing-edge down symmetric elevon deflections, is shown in figure 3. The total drag coefficient of the vehicle at a given Mach number, not counting the drag due to angle of attack and rudder, is given by the upper curve. At higher Mach numbers the drag increment of the elevons at 20° deflection is significant and is of the same order as the drag increment of the vehicle. Data in reference 15 show that for trailing edge down symmetric deflections greater than 20° the drag increment exceeds that of the basic vehicle.

The trend shown in figure 3 is characteristic of hypersonic vehicles controlled by aerodynamic control surfaces; for example, the shuttle orbiter (ref. 11). These trends of significant drag created by deflected control surfaces suggest that minimizing control deflections and control deflection bias for trim, especially at high Mach numbers, can significantly reduce the total drag of the vehicle.

Fuel Consumed Due to Elevon Drag In the study reported in reference 12 it was found that for the present configuration the fuel consumption due to elevon drag for the 1000 lb/ft<sup>2</sup> and 2000 lb/ft<sup>2</sup> reference trajectories was excessive. For these two cases the altitude above the earth as a function of time since takeoff is shown in figure 4; engine shutdown comes at approximately 1100 seconds after takeoff for the 2000 lb/ft<sup>2</sup> case and at 2400 seconds for the 1000 lb/ft<sup>2</sup> case. The weight of fuel used along these two paths as a function of flight Mach number is shown in figure 6. The fuel consumption due to elevon drag alone exceeds 17,000 lbs along the 1000 lb/ft<sup>2</sup> path and 6,500 lbs along the 2000 lb/ft<sup>2</sup> trajectory.

One reason for the unacceptable fuel consumption is the significant drag associated with use of elevons for trim as discussed above. Mach histories of the elevon deflections, presented in figure 5, show that maximum deflection bias reaches 12° trailing edge down in the 2000 lb/ft<sup>2</sup> case and

16° in the 1000 lb/ft<sup>2</sup> case. Bigger elevon deflections are required in the 1000 lb/ft<sup>2</sup> case because the trim angle of attack is approximately twice that of the 2000 lb/ft<sup>2</sup> case and this leads to a greater trim moment to counteract. Additionally, the 1000 lb/ft<sup>2</sup> case uses more fuel because the elevons remain deflected for a longer time and the ascent takes almost twice as long.

The excessive fuel consumption caused by the relatively small trim deflections of the elevons suggests that using aerodynamic control surfaces for trim moment generation in SSTO class vehicles may not be practical. This realization led to the investigation of the potential benefit of c.g. control to reduce trim moments and thrust vectoring to produce part of the required trim moments.

Potential Benefits of c.g. Control The magnitude of the undesired trim moments can be reduced if the vehicle c.g. position is actively controlled, so that the lift force passes approximately through the c.g. Decreasing the undesired trim moments would result in reductions in elevon deflection bias and consequently, fuel consumption. Conceptually, the c.g. could be controlled by selective depletion of remaining fuel; however, the issue under consideration in this study is not how to control the c.g., but rather what the benefit would be of controlling the c.g. If c.g. control is shown to be beneficial, then implementation scheme and trade-off studies could be performed.

Potential Benefits of Vectored Thrust Active control of propulsion system thrust direction can generate all or some of the trim moments needed. Used in this fashion, thrust vectoring trim control should result in decreased elevon deflection bias and could result in reduced fuel consumption. Active control of propulsion system thrust direction could be implemented by controlling the airbreathing engine geometry or by utilizing a vectorable rocket propulsion system. As in the case of c.g. control, the issue under consideration is not how to control the thrust direction but rather what is the benefit of controlling the thrust direction.

## RESULTS AND DISCUSSION

The c.g. position control and the thrust vectoring concepts described above are evaluated independently by comparing the ascent-to-orbit fuel consumed for each concept to the fuel consumed while using the baseline vehicle, elevon trim alone. Evaluations are performed for both reference trajectories. The six degrees-of-freedom simulation used for the analysis is described in Appendix B.

c.g. Control System Implementation The method used to control the c.g. was to override the baseline table of c.g. position (as a function of vehicle weight) and set the c.g. position equal to the

predetermined location of the a.c. as a function of flight Mach number as

$$x_{cg \text{ command}} = x_{ac}(M)$$

In the simulation it was assumed that the c.g. could track the estimated aerodynamic center position, and it was assumed that the "c.g. control system" hardware weight was negligible.

Elevon Deflections with c.g. Position Control The left elevon deflection angle as a function of Mach number for the 1000 lb/ft<sup>2</sup> and 2000 lb/ft<sup>2</sup> maximum dynamic pressure ascents with and without c.g. position control are shown in figure 7. The right elevon deflection angle history is for all practical purposes the same and is not depicted. The instantaneous mean value is basically the deflection bias required to produce the trim moment to hold the vehicle at the desired angle of attack.

Without c.g. position control the relatively large deflections above Mach 5 are not desirable, and as was shown previously, these deflections cause unacceptably high drag and increased fuel consumption. Causing the c.g. to track the a.c. reduces the moments required to hold the vehicle at desired angles of attack and reduces the elevon deflection bias to the -2 to 2° range. As will be demonstrated, reducing the elevon deflection bias significantly reduces the fuel consumed to orbit.

The unrealistic magnitudes of the elevon angles, above Mach 22, were used to perform the pitch-up maneuver computed to enter the transfer orbit. After this maneuver, dynamic pressure decreases rapidly and aerodynamic control effectiveness is lost. These elevon deflections are an artifact of the simulation; they produced very little drag due to the low dynamic pressure, and consequently, insignificant fuel penalty. In an actual vehicle, a reaction control system would be used to provide attitude control during the transfer orbit coast phase.

Fuel Consumption with c.g. Control The effect on fuel consumption of the c.g. tracking the a.c. is shown in figure 8. The total fuel consumption to orbit for the 1000 lb/ft<sup>2</sup> and 2000 lb/ft<sup>2</sup> maximum dynamic pressure ascents with and without c.g. control are plotted as a function of time after takeoff. The time scale on the figure is started at 1000 seconds and the fuel consumed scale is started at 140,000 lbs so the differences in fuel consumption are easier to show. The horizontal portions of the curves correspond to the engine-off coast phase of the ascent.

The reduced elevon deflections decreases the drag of the elevons and hence the total drag of the vehicle. The decreased drag results in reduced thrust required to maintain the desired flight path. As shown in figure 8 this drag reduction decreases fuel consumption by more than 3000 lbs fuel along the 2000 lb/ft<sup>2</sup> path and more than 6000 lbs along the 1000 lb/ft<sup>2</sup> path.

It is noted that the full amount of fuel attributed to elevon drag shown in figure 5 is not saved because the vehicle flies at a slightly higher angle of attack to compensate for the slight loss of lift caused by smaller deflections of the elevons. The higher angle of attack produces slightly more fuselage and wing pressure drag than in the baseline case and therefore, nullifies some of the benefit derived from the reduced elevon deflections.

The fairly significant fuel savings over the baseline attributed to the c.g. tracking the a.c. indicates the potential of maintaining neutral aerodynamic stability through c.g. control and/or configuration control and design in horizontal takeoff SSTO launch vehicles. Neutral longitudinal stability has the advantage of minimizing aerodynamic trim moments and reducing control deflections needed to maneuver the vehicle. The required dynamic stability and handling qualities can be provided by an automatic flight control system.

Effect of Thrust Vectoring To evaluate the thrust vectoring concept, the total fuel consumed with thrust vectoring is compared to that of the baseline using the same six degrees-of-freedom simulation of the two ascents used in the c.g. control study. It is assumed that the "thrust vectoring control system" has sufficient authority to counteract the aerodynamic forces and keep the elevon deflections close to 0°, and it is also assumed that the thrust vectoring does not decrease the efficiency of the propulsion system. However, the thrust along the body x-axis is reduced by the cosine of the thrust vector angle. Finally, it is assumed that the thrust vectoring control system adds negligible weight.

The method used to simulate thrust vector control is to gimbal the thrust vector in proportion to the integral of the symmetric elevon angle as given by

$$\delta_T = K_T \int_0^t \delta_{ELE} dt$$

where the gimballed thrust is assumed to act at the aft end of the fuselage. This control law is designed to keep the symmetric elevon angle close to zero.

The effect of thrust vectoring trim control on elevon deflections for the 1000 lb/ft<sup>2</sup> and 2000 lb/ft<sup>2</sup> maximum dynamic pressure ascents is shown in figure 9. The independent variable is the flight Mach number. The lower curves are for the baseline without thrust vector control. The use of thrust vector control generates most of the required trim moment and reduces the elevon deflections for trim to the -2° to 2° range throughout the Mach range.

The thrust vector angle required for trim as a function of flight Mach number for the 1000 lb/ft<sup>2</sup> and 2000 lb/ft<sup>2</sup> ascents is shown in figure 10. The values above the zero deflection line correspond to a nose down moment. The greatest thrust vector angles occur with the 1000 lb/ft<sup>2</sup> case because this case flew at a higher angle of attack resulting in a larger trim moment coefficient.

In the simulation the engines were shut down at Mach 24.2 to begin the coast to the desired apogee; beyond this Mach number the elevons provided all of the trim moment required. The increase in computed thrust vector angle beyond this Mach number is caused by the control law that integrated the elevon angle to obtain the desired thrust angle. As in the c.g. control case, in an actual vehicle a reaction jet control system would be used to maintain attitude control during the coast phase.

The effect of thrust vector trim control on fuel consumption is shown in figure 11. The two curves on the left give the total fuel consumption for the 2000 lb/ft<sup>2</sup> maximum dynamic pressure ascent, and the two on the right are for the 1000 lb/ft<sup>2</sup> case. In all four cases the independent variable is elapsed time since takeoff.

In both cases thrust vectoring saves significant fuel over the baseline. As demonstrated earlier, actively controlling the thrust vector angle so as to minimize the lift and drag moment keeps the elevon deflections in the -2° to 2° range. The reduced deflection reduces the drag of the elevons and hence the total drag of the vehicle. The drag reduction results in reduced thrust and fuel consumption rate needed to maintain the desired flight path; this saves approximately 2800 lbs of fuel along the 2000 lb/ft<sup>2</sup> path and 5500 lbs along the 1000 lb/ft<sup>2</sup> path.

As in the c.g. control case these results also illustrate that the full amount of fuel consumption attributed to elevon drag shown earlier is not saved because the vehicle flies at a slightly higher angle of attack to compensate for loss of lift caused by reduced elevon deflections. The fairly significant fuel savings over the baseline vehicle attributed to the thrust vectoring control system indicate the potential of thrust vector control in this class of launch vehicles.

This study addresses a configuration where the baseline thrust vector passes through the c.g. Consider the more general case where the baseline thrust vector passes above or below the c.g. The results presented in this section indicate that having the thrust vector above the c.g. decreases the trim moment requirement for an aerodynamically unstable configuration and increases it for an stable configuration; having the thrust vector below the c.g. has the opposite effect. This fact is important since it indicates that trim drag can be decreased by proper alignment of the thrust vector in the design process.

Combined Stability Augmentation, c.g. Control, and Thrust Vectoring Based on the favorable evaluations of c.g. control and thrust vectoring control as possible means of reducing trim drag, the two concepts were integrated and tested. The c.g. control system was given one-half the authority needed to cause the c.g. to track the a.c., and the thrust vectoring system was used to provide the remaining moment needed to keep the mean elevon angles close to zero. A guidance and stability augmentation system was used as before to provide dynamic stability and tracking of the desired precomputed paths.

With the combined system no significant improvement in fuel savings over the individual systems was found, and the thrust vector angles, as expected, reached one-half the values obtained when thrust vectoring was used alone. The practical benefit of integrating the two concepts lies in the fact that in practice, c.g. and thrust vectoring control systems would have limited authority and together the capacity of the total system would be increased.

Effect of Propulsion System on Vehicle Stability Hypersonic propulsion systems can significantly affect the stability of the vehicle. It is shown in reference 16 that at hypersonic speeds the thrust coefficient can change by more than 10 percent per degree change of angle of attack. In a typical underslung scramjet system an increase in angle of attack increases the engine capture area which equates to an increase in the total mass of air captured by the inlet, thereby decreasing the equivalence ratio. Even though the capture area increases, the resulting decrease in equivalence ratio will more than likely reduce the net thrust and thereby cause a stable nose down moment (provided that the thrust vector passes below the vehicle c.g.). If the fuel flow rate is increased as the angle of attack is increased, such that the equivalence ratio remains constant, then an increase in thrust would be expected due to the increased capture area. This thrust increase with angle of attack would then result in an unstable nose up moment. Thus, it is seen that the vehicle becomes either more or less stable depending on how the fuel flow is controlled and whether or not the thrust vector passes above or below the c.g.

## CONCLUDING REMARKS

A study of trim drag reduction concepts for a generic horizontal-takeoff single-stage-to-orbit (SSTO) vehicle has resulted in the following findings.

1. The aerodynamic center migrates forward a significant fraction of fuselage length as the flight Mach number increases to orbital values, and this migration causes aerodynamic instability and unacceptably large changes in longitudinal trim moments.
2. Use of elevons to counteract the trim moments results in a moderate elevon deflection bias and an increase in drag which leads to excessive fuel consumption.
3. Controlling the c.g. location so it tracks the vehicle a.c. yields a more neutrally stable configuration, reduces trim moment requirements and elevon deflection bias, increases control power, and results in significant fuel savings.
4. Controlling the direction of the thrust vector to produce trim moments decreases elevon deflection bias and also results in significant fuel savings.
5. The combination of active c.g. position control to improve stability and minimize trim moment requirements and thrust vectoring control to generate trim moments has the potential to minimize trim drag and significantly reduce the ascent fuel consumption for horizontal-takeoff SSTO vehicles.

## REFERENCES

1. Freeman, D. C., et al.: The Future Space Transportation System (FSTS) Study. *Astronautics and Aeronautics*, Vol. 21, No. 6, June 1983.
2. Talay, T.A., and Morris, W.D.: Advanced Manned Launch Systems. EAC Paper EAC '89-17, AAAF/DGLR/RAeS/ESA Second European Aerospace Conference Progress in Space Transportation, Bonn - Bad Godesberg, Federal Republic of Germany, 1989.
3. Piland, W. M., and Talay, T. A.: Advanced Manned Launch Systems Comparisons. IAF Paper 89-121, 40th Congress of the International Astronautical Federation, Malaga, Spain.
4. Martin, J. A., et al. : "Orbit on Demand: In This Century If Pushed." *Astronautics and Aeronautics*, Vol. 23, No. 2, February 1985.
5. Hahne, David E.; Luckring, James M.; Covell, Peter F.; Phillips, W. Pelham; Gatlin, Gregory M.; Shaughnessy, John D.; and Nguyen, Luat T.: Stability Characteristics of a Conical Aerospace Plane Concept. SAE Paper No. 892313, Aerospace Technology Conference and Exposition, Anaheim, California, September 25-28, 1989.
6. Phillips, W. P.; Brauckmann, G. J.; Micol, J. R.; and Woods, W. C.: Experimental Investigation of the Aerodynamic Characteristics for a Winged-Cone Concept. AIAA Paper No. 87-2484, 5th Applied Aerodynamics Conference, Monterey, California, August 17-19, 1987.
7. Fox, C. H. Jr.; Luckring, J. M.; Morgan, H. L., Jr.; and Huffman, J. K.: Subsonic Longitudinal and Lateral-Directional Static Aerodynamic Characteristics of a Slender Wing-Body Configuration. NASP TM-1011, 1988.
8. Shaughnessy, John D.; and Sliwa, Steven M.: Preliminary Stability and Control Analysis for Aerospace Plane Configurations. Paper No. 42, Third NASP Technology Symposium, NASP CP 3018, Vol. III NASA Ames Research Center, Moffett Field California, June 2-4, 1987, pp. 145-166.
9. Shaughnessy, John D.; and Roy, Marie-Louise: Longitudinal Stability and Control Power Analysis of an Aero-Space Plane Configuration. NASP TM-1009, September 1987.

10. Penland, Jim A.; Hallissy, James B.; and Dillon, James L.: Aerodynamic Characteristics of a Hypersonic Research Airplane Concept Having a 70° Swept Double-Delta Wing at Mach Numbers From 0.80 to 1.20 With Summary Data From 0.20 to 6.0. NASA TP-1552, December 1979.
11. Operational Aerodynamic Data Book, Vol 3, Orbiter Vehicle Aerodynamic Data. STS85 0118, September 1985.
12. Shaughnessy, John D.; Powell, Richard W.; Kelley, Marie-Louise; and Leath, William J. Jr.: A Six Degrees-of-Freedom Analysis of the Ascent Phase of a Generic Hypersonic Vehicle. Paper No. 53, Fifth NASP Technology Symposium, NASP CP-5030, Vol. III. NASA Langley Research Center, Hampton, Virginia, October 18-21, 1988, pp. 115-141.
13. Sova, G., and Divan, P. : Aerodynamic Preliminary Analysis System II, Part II, User's Manual. NASA CR-182077, 1991.
14. Pinckney, S. Z.: Internal Performance Predictions for Langley Scramjet Engine Module. NASA TM X-74038, January 1978.
15. Shaughnessy, John D.; Pinckney, S. Zane; McMinn, J. Dana; Cruz, Christopher, I.; and Kelley, Marie-Louise: Hypersonic Vehicle Simulation Model: Winged-Cone Configuration . NASA TM-102610, 1990.
16. Walton, J.: Performance Sensitivity of Hypersonic Vehicles to Changes in Angle of Attack and Dynamic Pressure. AIAA 89-2463, 1989.
17. Brauer, G. L.; Cornick, D. E.; and Stevenson, R.: Capabilities and Applications of the Program to Optimize Simulated Trajectories (POST). NASA CR-2770, February 1977.

TABLE I.- GEOMETRIC CHARACTERISTICS OF CONFIGURATION

Wing:

Reference area (includes area projected to fuselage centerline), ft <sup>2</sup> .....	3603
Aspect ratio.....	1.00
Span, ft.....	60.0
Leading edge sweep angle, deg.....	75.97
Trailing edge sweep angle, deg.....	0.0
Mean aerodynamic chord, ft.....	80.0
Airfoil section.....	diamond
Airfoil thickness to chord ratio, percent.....	4.0
Incidence angle, deg.....	0.0
Dihedral angle, deg.....	0.0

Wing flap (elevon):

Area each, ft <sup>2</sup> .....	92.3
Chord (constant), ft .....	7.22
Inboard section span location, ft .....	15.0
Outboard section span location, ft .....	27.78

Vertical tail, body centerline:

Exposed area, ft <sup>2</sup> .....	645.7
Theoretical area, ft <sup>2</sup> .....	1248.8
Span, ft.....	32.48
Leading edge sweep angle, deg.....	70.0
Trailing edge sweep angle, deg.....	38.13
Airfoil section.....	diamond
Airfoil thickness to chord ratio, percent.....	4.0

TABLE I.- CONCLUDED

Rudder:

Area, ft <sup>2</sup> .....	161.4
Span, ft.....	22.8
Chord to vertical tail chord ratio, percent.....	25.0

Canard:

Exposed area, ft <sup>2</sup> .....	154.3
Theoretical aspect ratio.....	5.48
Span, ft.....	33.6
Leading edge sweep angle, deg.....	16.0
Trailing edge sweep angle, deg.....	0.0
Airfoil section.....	NACA 65A006
Incidence angle, deg.....	0.0
Dihedral angle, deg.....	0.0

Axisymmetric fuselage:

Theoretical length, ft.....	200.0
Cone half angle, deg.....	5.0
Cylinder radius (maximum), ft.....	12.87
Cylinder length, ft.....	12.88
Boattail half angle, deg.....	9.0
Boattail length, ft.....	40.0
Moment reference center, ft.....	124.01

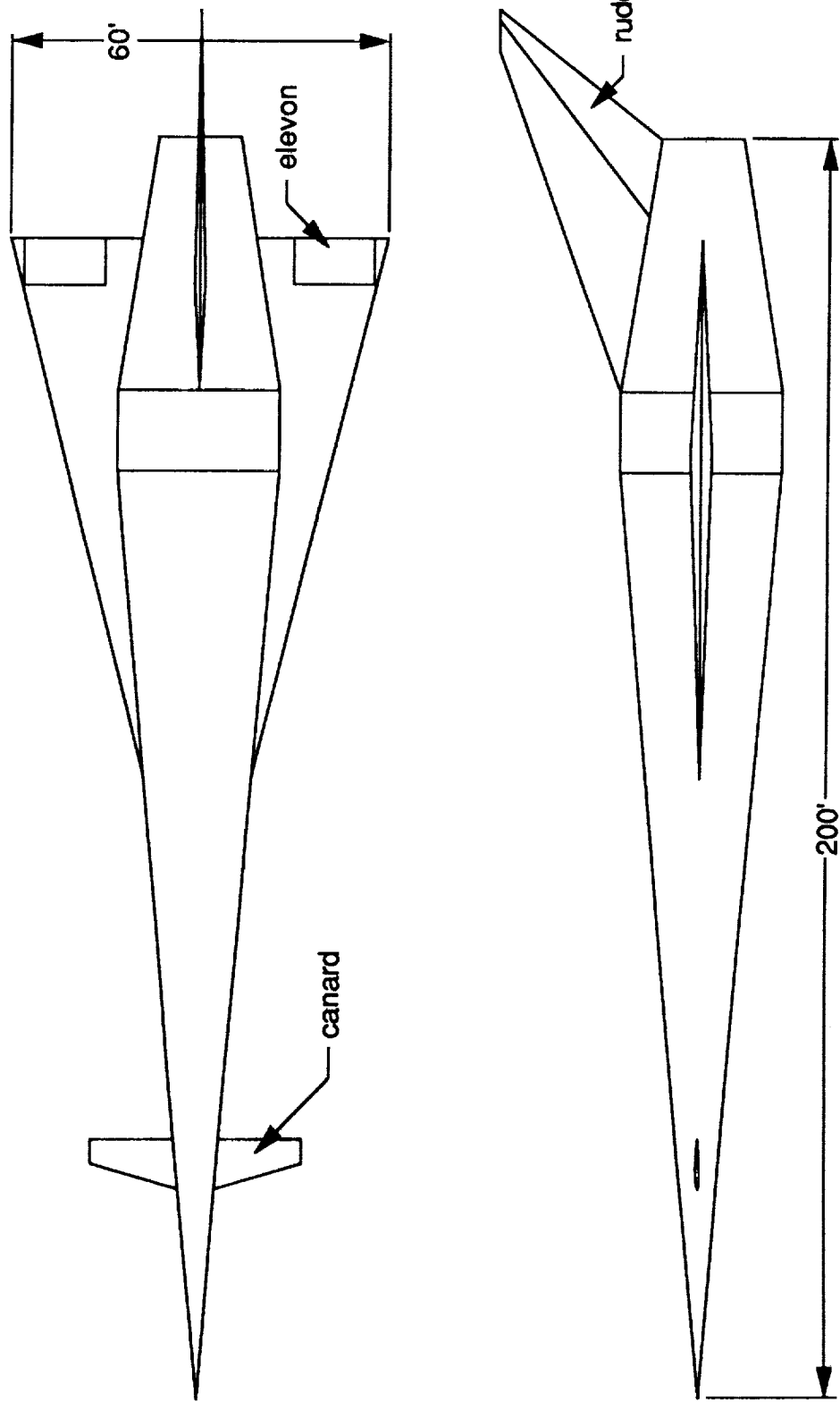


Figure 1.- Configuration geometry

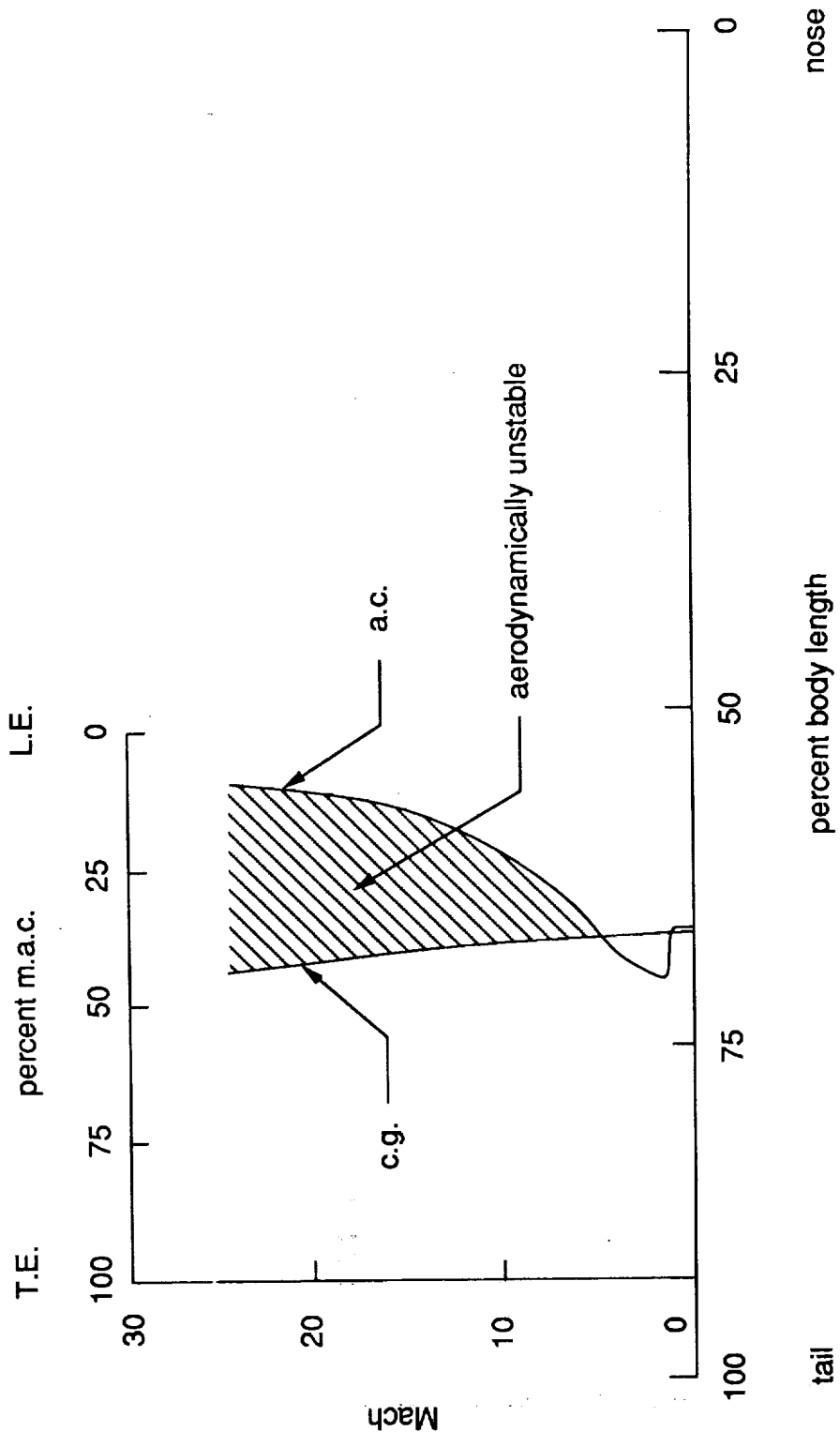


Figure 2.- Aerodynamic center and center of gravity of study configuration

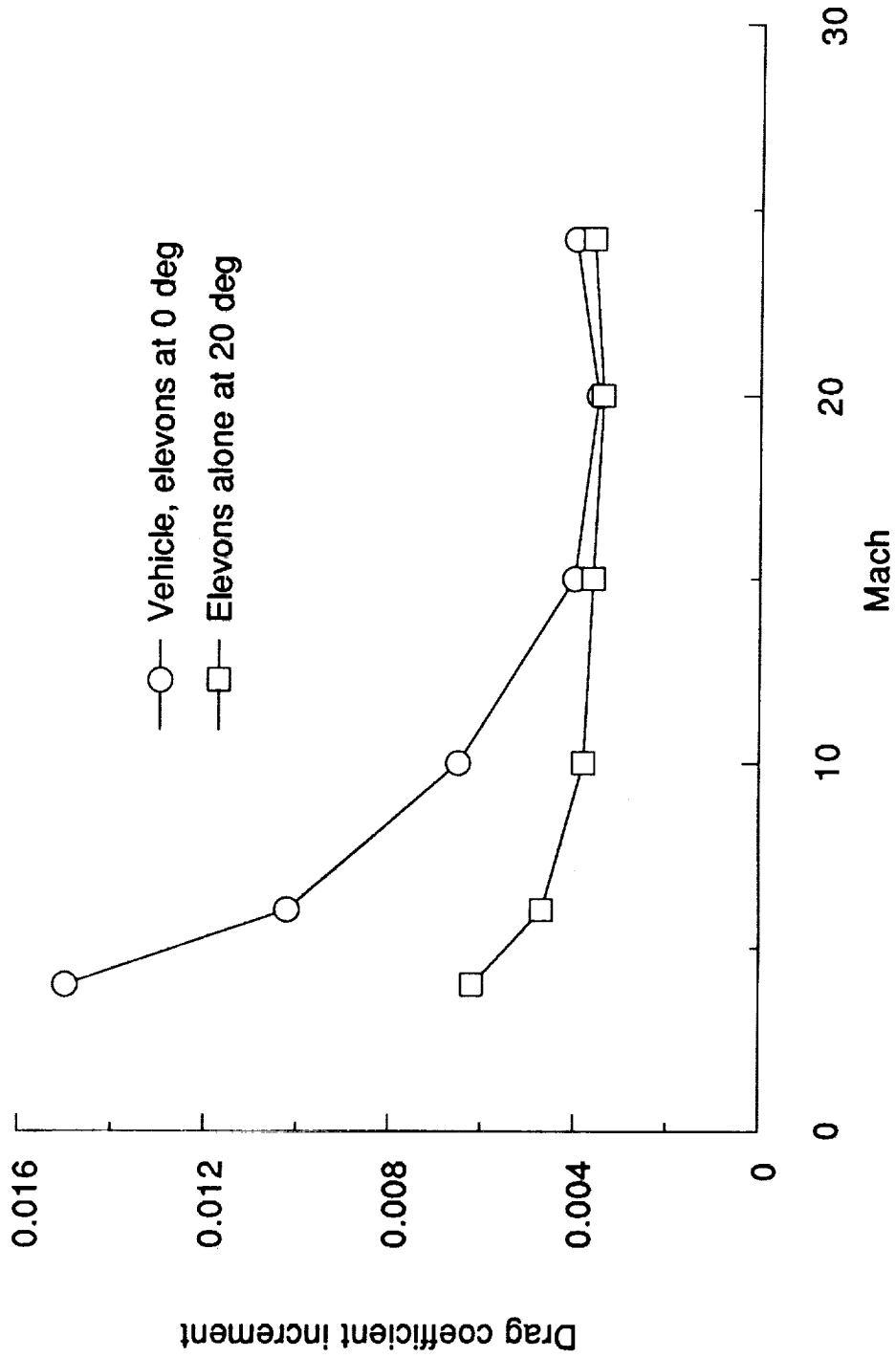


Figure 3.- Drag of deflected elevons compared to drag of entire vehicle at zero angle of attack

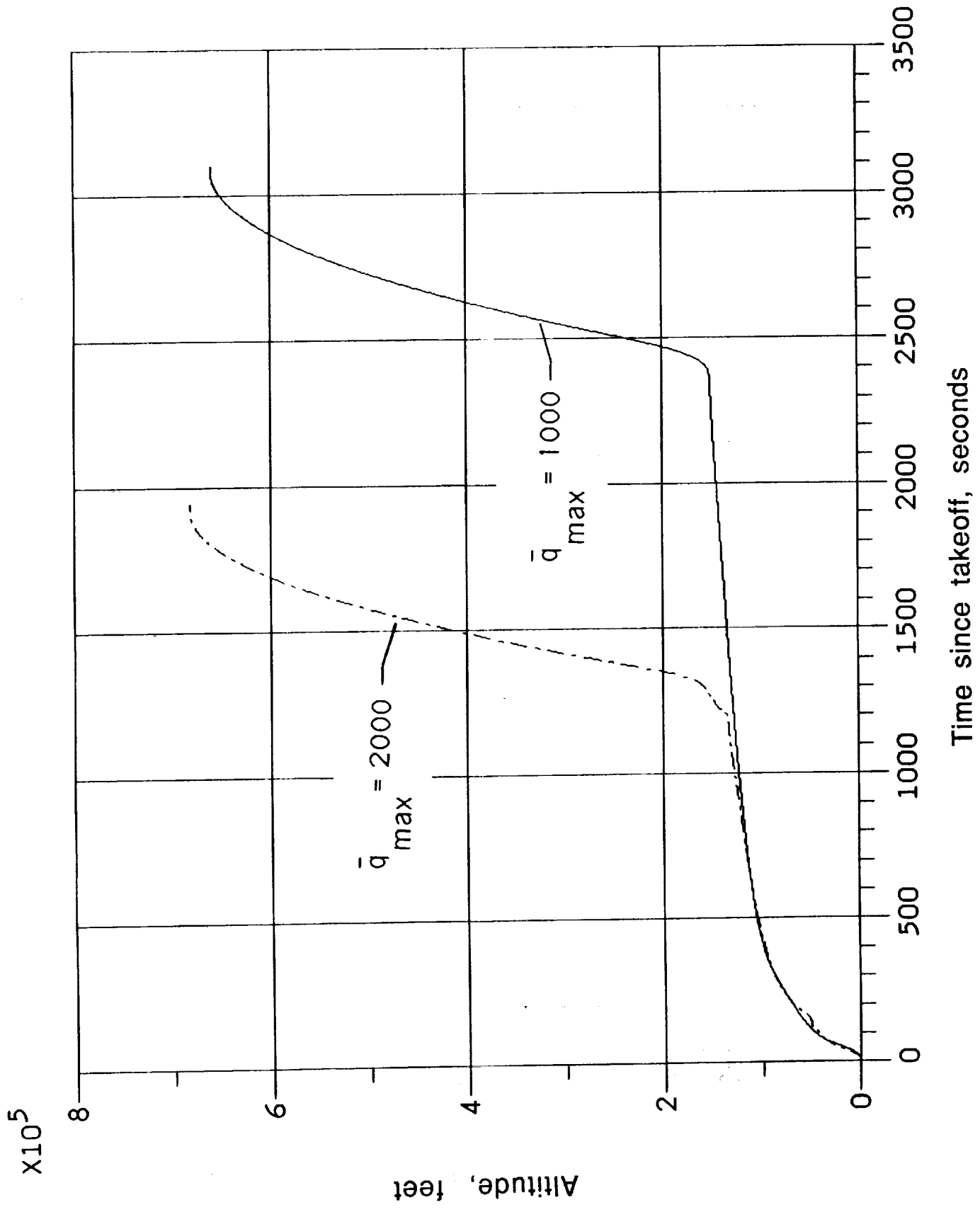


Figure 4.- Altitude above the earth as a function of time for 1000 psf and 2000 psf maximum dynamic pressure trajectories.

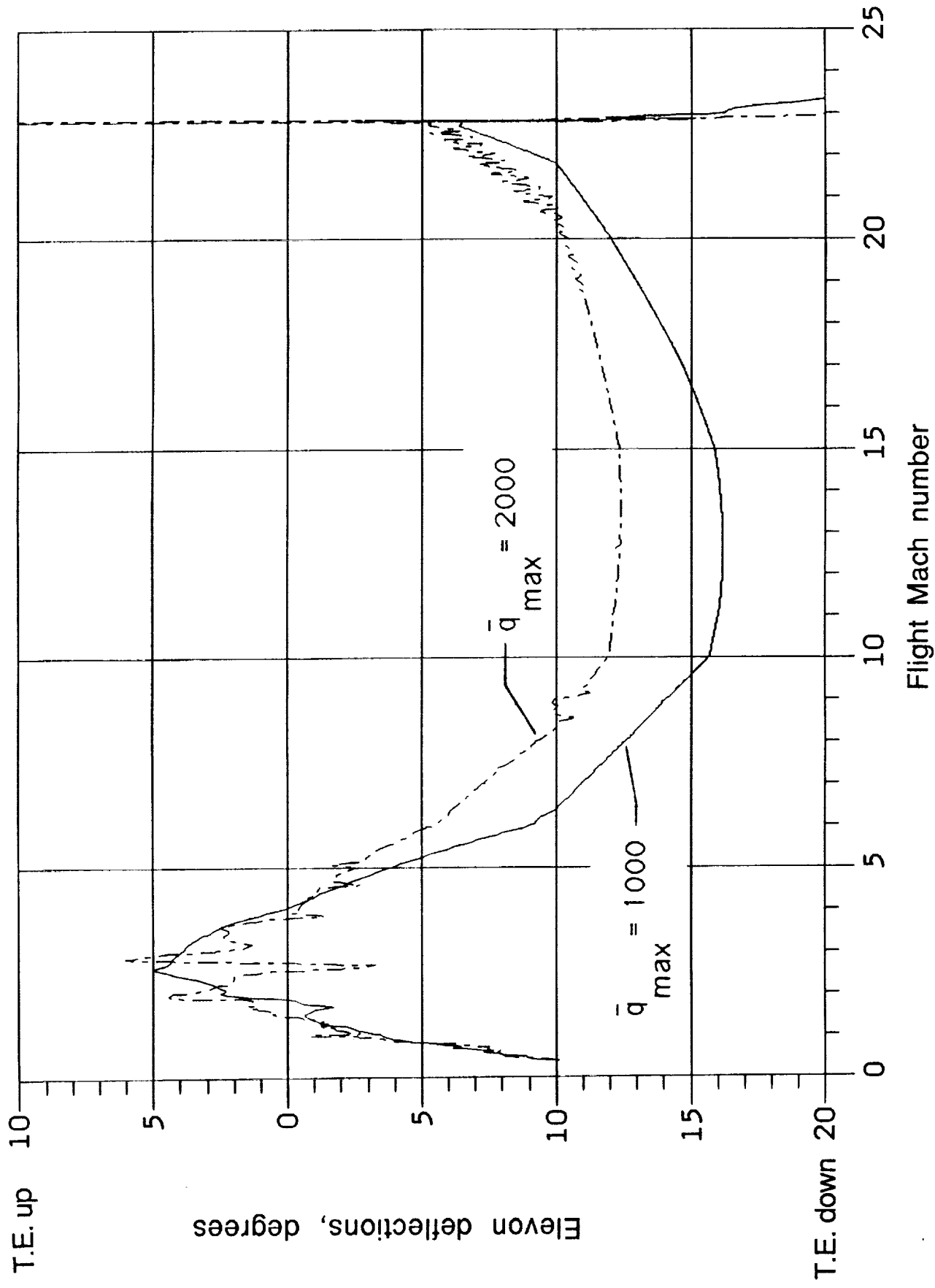


Figure 5.- Elevon deflections as a function of flight Mach number for 1000 psf and 2000 psf maximum dynamic pressure trajectories.

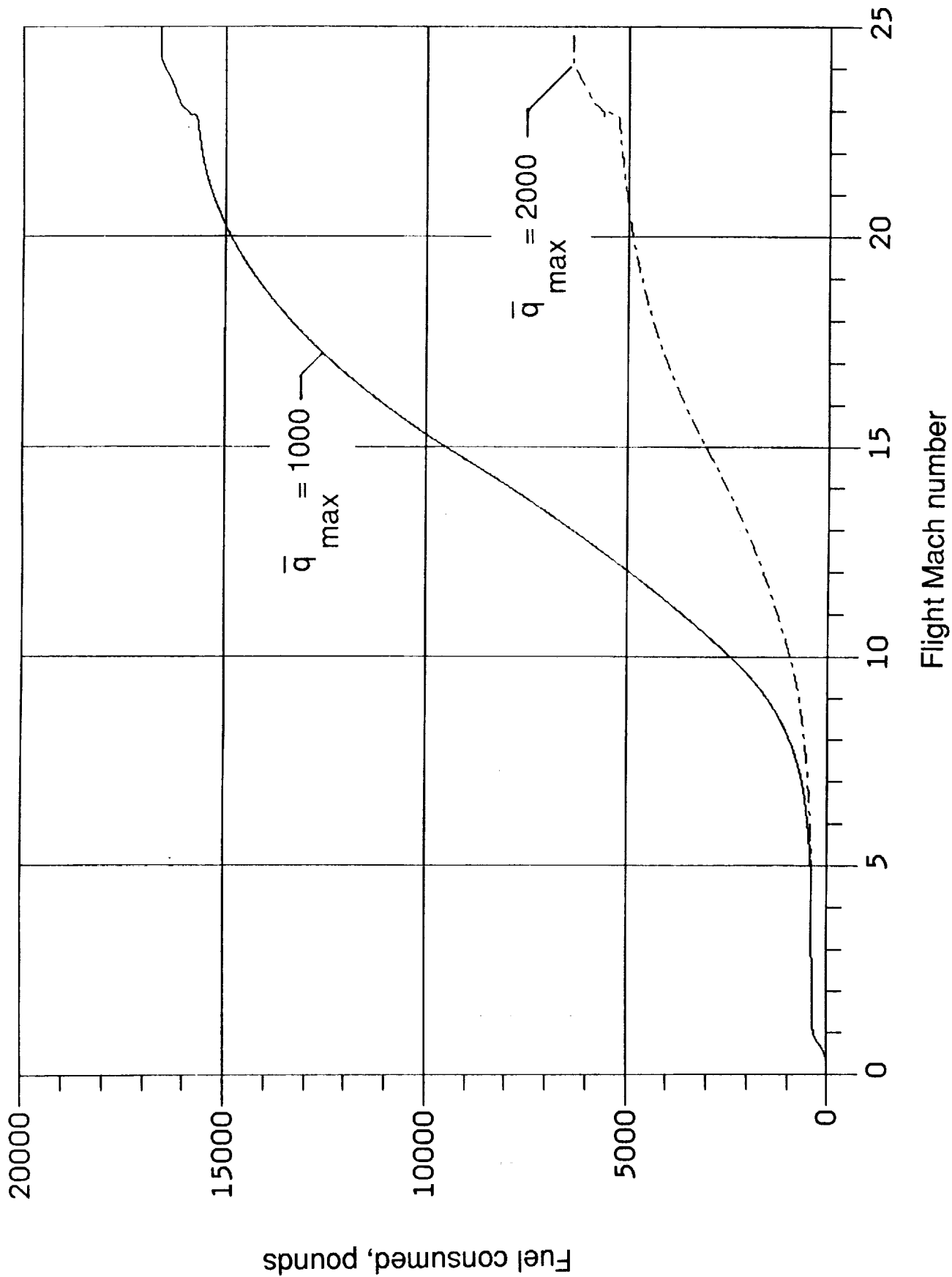


Figure 6.- Fuel consumed due to elevon drag for 1000 psf and 2000 psf maximum dynamic pressure trajectories.

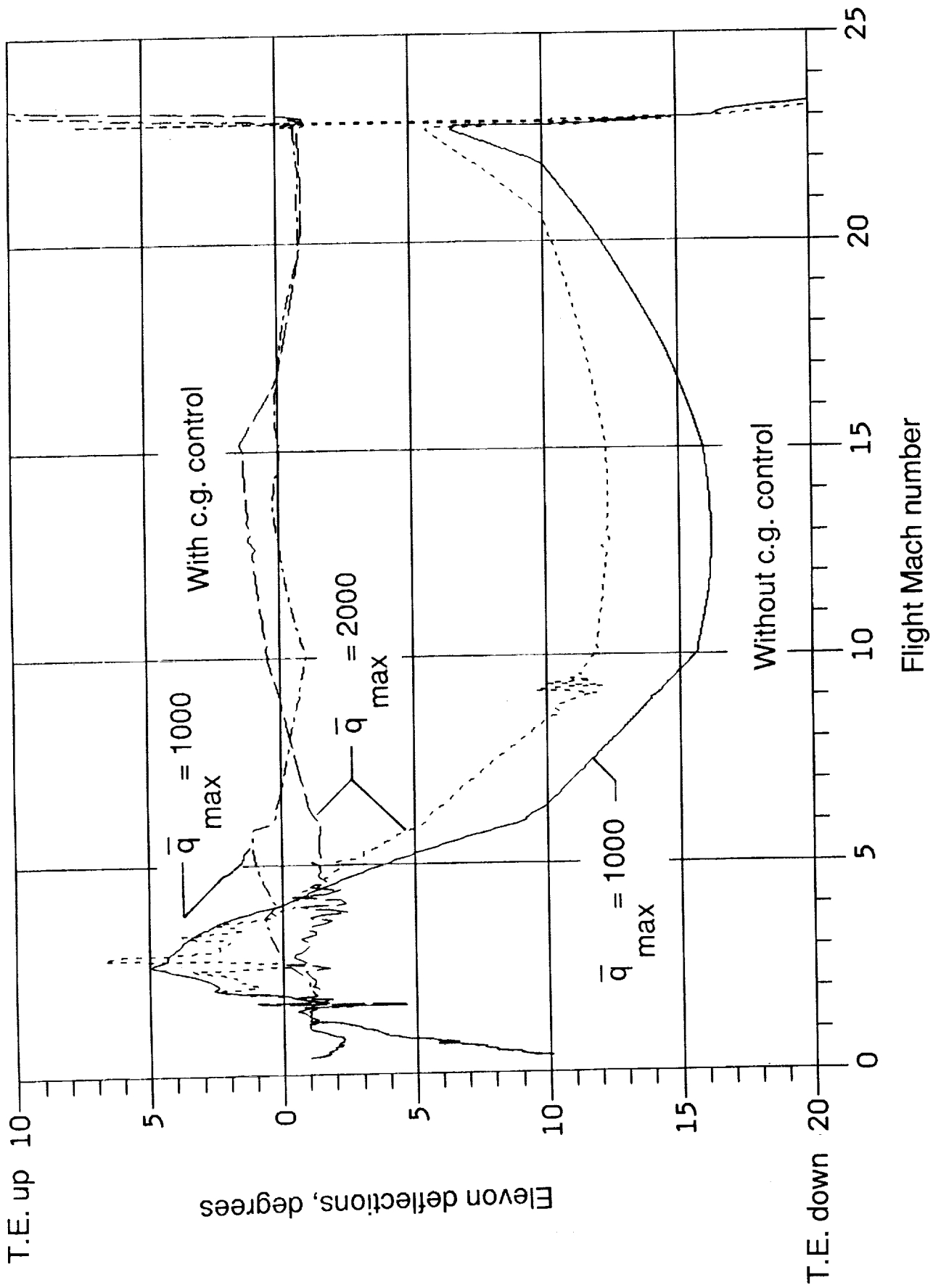


Figure 7.- Elevon deflections as a function of flight Mach number with and without c.g. control for 1000 psf and 2000 psf maximum dynamic pressure trajectories.

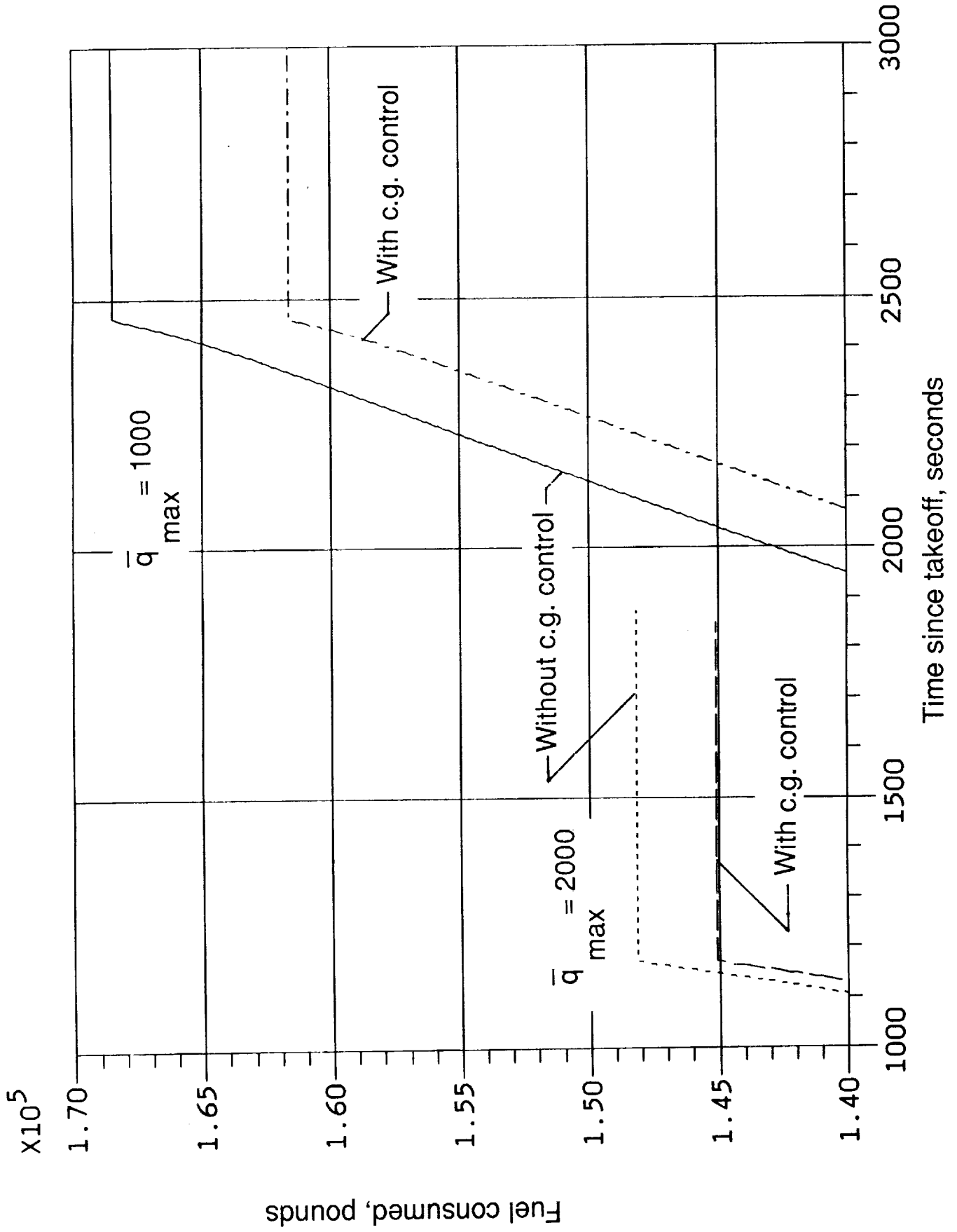


Figure 8.- Fuel consumed as a function of time since takeoff with and without c.g. control for 1000 psf and 2000 psf maximum dynamic pressure trajectories.

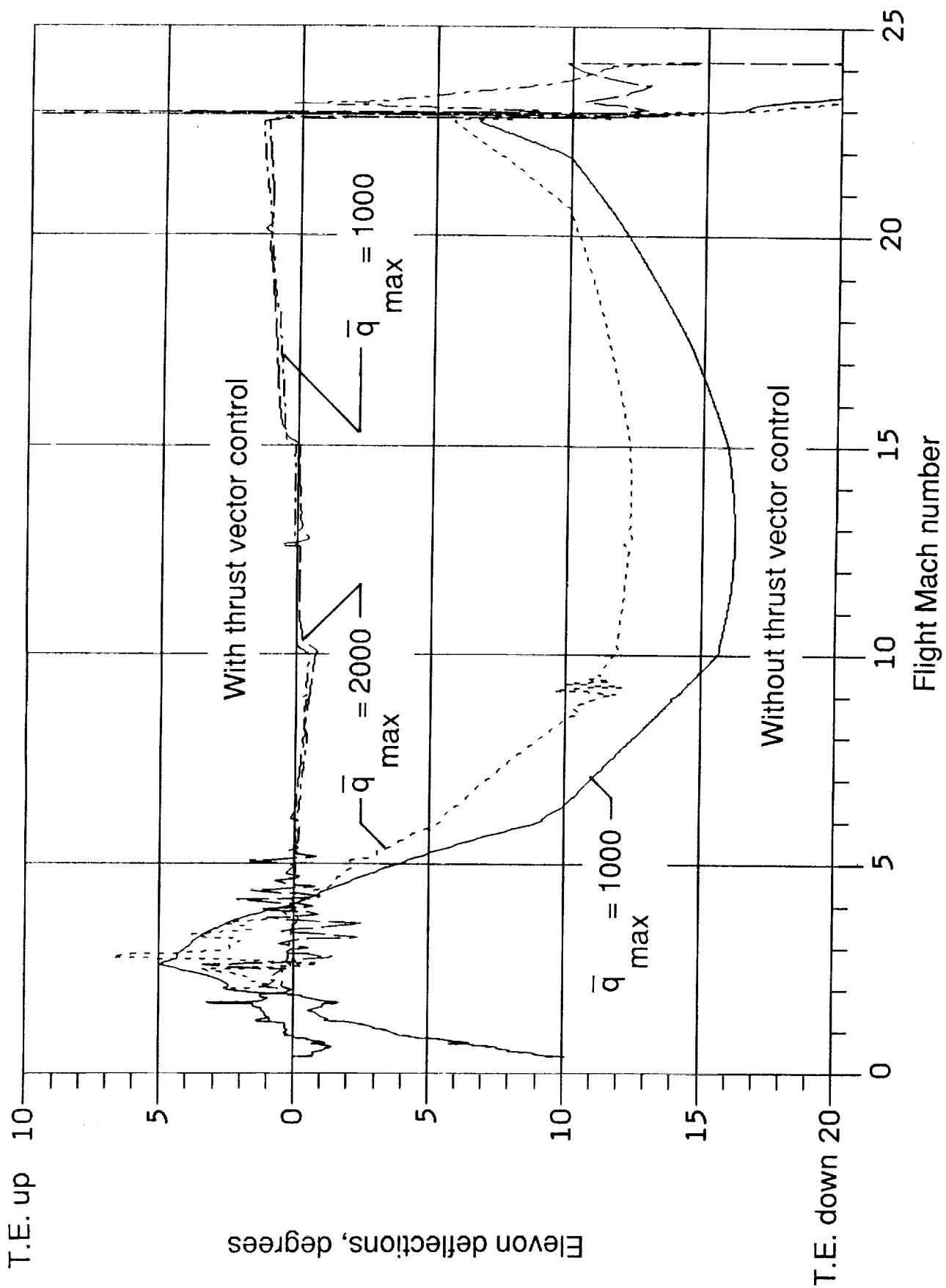


Figure 9.- Elevon deflections as a function of flight Mach number with and without thrust vector control for 1000 psf and 2000 psf maximum dynamic pressure trajectories.

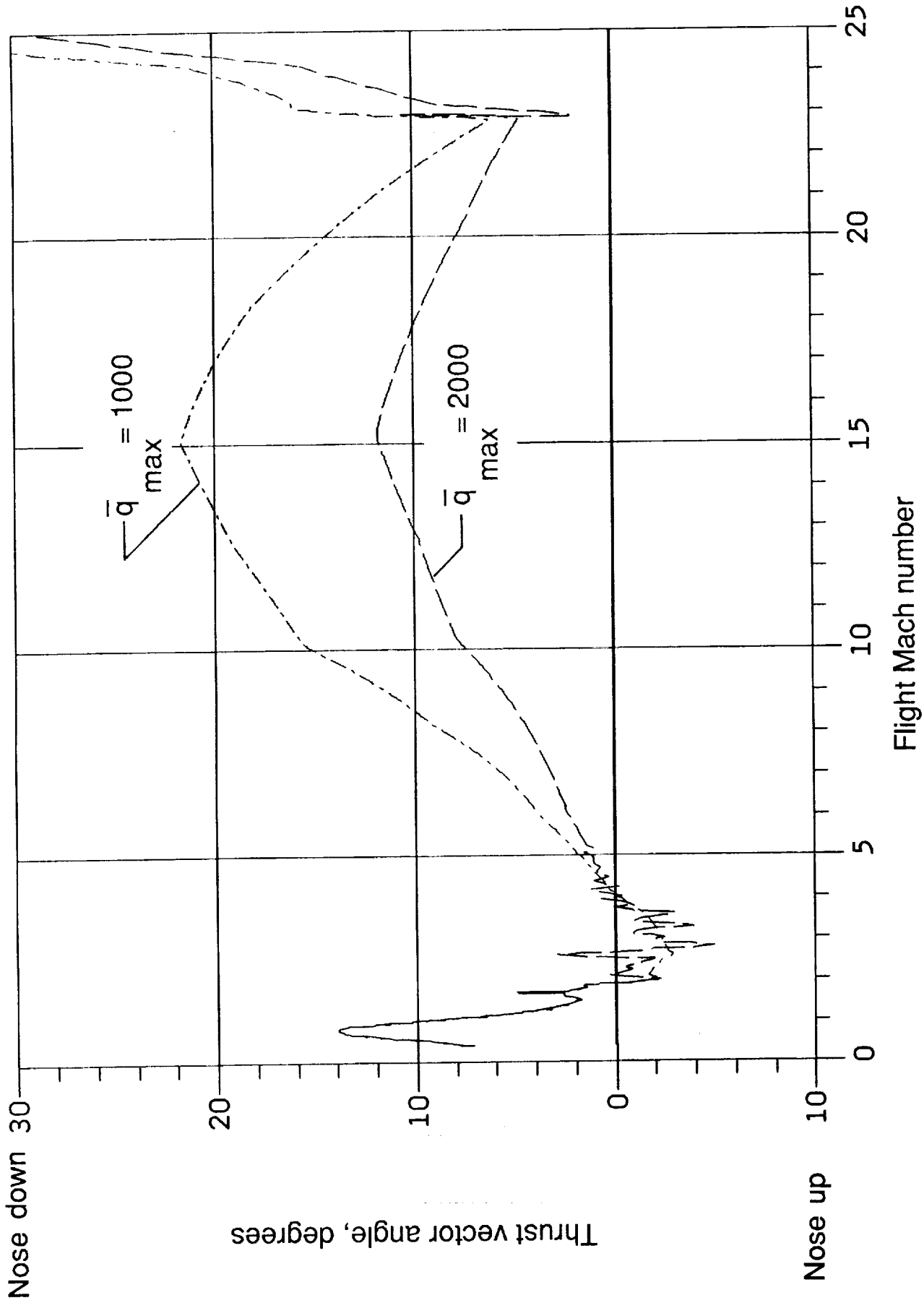


Figure 10.- Thrust vector turning angle as a function of flight Mach number for 1000 psf and 2000 psf maximum dynamic pressure trajectories.

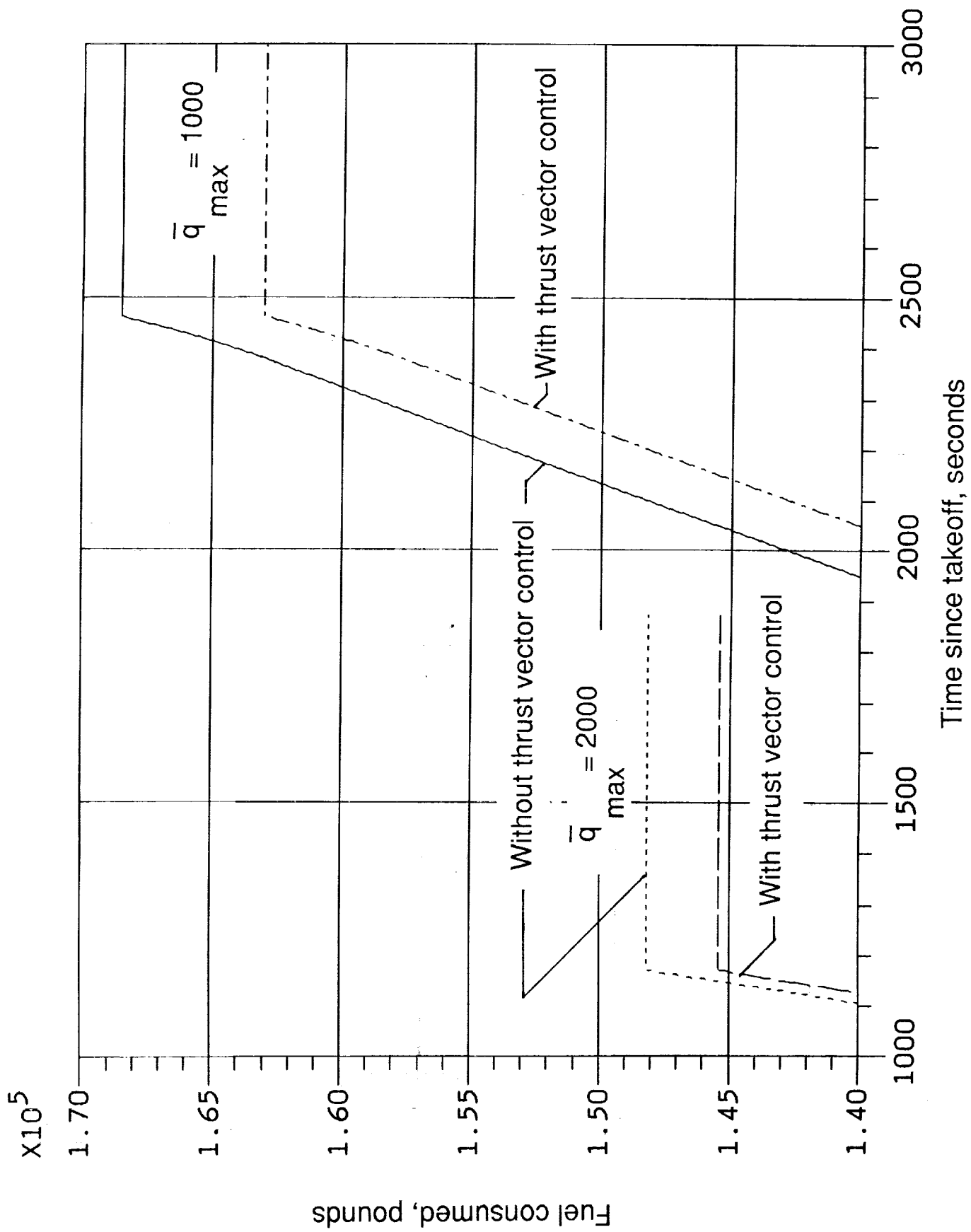


Figure 11.- Fuel consumed as a function of time since takeoff with and without thrust vector control for 1000 psf and 2000 psf maximum dynamic pressure trajectories.

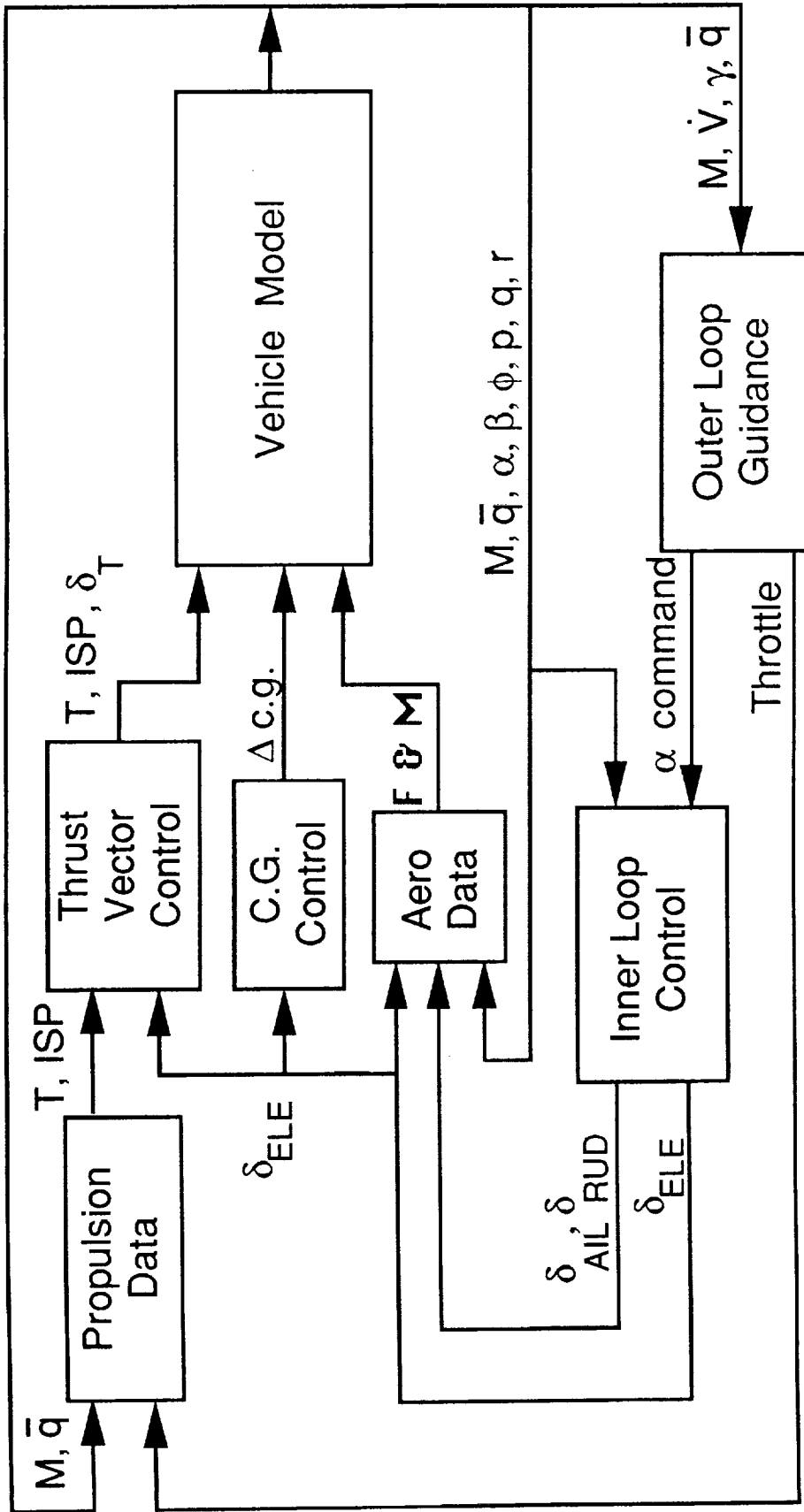


Figure 12.- Simulation block diagram.

## Appendix A

### Vehicle Simulation Models

This appendix describes conceptually the aerodynamics, propulsion, and mass models for a generic slender winged-cone hypersonic vehicle. The models and data are described in more detail in reference 15.

Aerodynamics Model Experimental aerodynamic data including control surface effectiveness and drag increments were not available across the Mach range so they were estimated. A subsonic-supersonic-hypersonic analysis code, referred to as the Aerodynamic Preliminary Analysis System (APAS) (ref. 13), was used to predict the longitudinal and lateral-directional force and moment coefficients. Data were estimated at Mach numbers from 0.3 to 24.2; angles of attack from  $-1.0^\circ$  to  $12.0^\circ$ ; right elevon, left elevon, and rudder deflections from  $-20.0^\circ$  to  $20.0^\circ$ ; and canard deflections from  $-10.0^\circ$  to  $10.0^\circ$ . The data were implemented in the simulation (described in Appendix B) as table look-up functions.

Propulsion Model The propulsion model used in the study was created by using a modified version of the cycle analysis method presented in reference 14. The thrust coefficient and specific impulse were determined as functions of Mach number from 0 to 25, dynamic pressure from 0 to  $5000 \text{ lb/ft}^2$ , and fuel equivalence ratio from 0 to 100. (These "end values" of dynamic pressure and equivalence ratio had no physical meaning and were used for programming convenience only.)

Mass Model The vehicle mass model is based on the assumption of distributed fuel and rigid structure; fuel slosh was not considered. The mass of the vehicle and its moments of inertia varied as fuel was consumed. The total weight of fuel consumed  $W_{\text{CON}}$  was obtained by integrating the fuel flow rate over the time the engines were thrusting as

$$W_{\text{CON}} = \int_0^t \dot{W} dt$$

where

$$\dot{W} = \frac{T}{I_{\text{sp}}}$$

The vehicle weight was then given by

$$W = W_0 - W_{CON}$$

where  $W_0$  is the initial weight of the vehicle. It is assumed that the c.g. moves only in the x-body axis direction as fuel is consumed. The c.g. location,  $x_{CG}$ , and the mass moments of inertia were implemented in the simulation as a table look-up functions of vehicle weight. The products of inertia are neglected.

## Appendix B

### Description of the Simulation

The block diagram of the simulation used in this study is shown in figure 12. The six degrees-of-freedom version of POST (ref. 17) was used as the simulation program. Standard symbols are used in the figure to represent the simulation variables.

The Vehicle Model block contains the vehicle equations of motion involving an oblate rotating Earth and standard atmosphere. A fourth-order Runge-Kutta integration algorithm with step size of 0.1 sec was used. Angles of attack and sideslip, Mach, and dynamic pressure from the Vehicle Model block are inputs to the Aero Data block that generated the basic aero forces and moments. Dynamic pressure, Mach, flight path angle, and acceleration, computed in the Vehicle Model block, are input to the Outer Loop Guidance block. This block contains the desired variation in dynamic pressure, flight path angle, and acceleration as a function of Mach number for two precomputed  $1000 \text{ lb/ft}^2$  and  $2000 \text{ lb/ft}^2$  maximum dynamic pressure trajectories. Algorithms in this block compute angle of attack and throttle commands as a function of errors in dynamic pressure, flight path angle, and acceleration. The command value of angle of attack is input to the Inner Loop Control block that provides artificial stability for the vehicle and causes the vehicle angle of attack to become equal to the command value. The Inner Loop Control block determines the elevon and rudder commands. These commands are input into the Aero Data block that computes the incremental forces and moments due to the aerosurface deflections. Symmetric elevon deflection input to the Thrust Vector Control and c.g. Control blocks determines the thrust vector angle and change in c.g. position, respectively, to minimize elevon deflection bias. Throttle command, Mach, and dynamic pressure are input to the Propulsion Data block, and this block generates the thrust and specific impulse that are passed to the Vehicle Model block. The fuel consumption data are computed in the Vehicle Model block.

# REPORT DOCUMENTATION PAGE

*Form Approved*  
OMB No. 0704-0188

Public reporting burden for this collection of information is estimated to average 1 hour per response, including the time for reviewing instructions, searching existing data sources, gathering and maintaining the data needed, and completing and reviewing the collection of information. Send comments regarding this burden estimate or any other aspect of this collection of information, including suggestions for reducing this burden, to Washington Headquarters Services, Directorate for Information Operations and Reports, 1215 Jefferson Davis Highway, Suite 1204, Arlington, VA 22202-4302, and to the Office of Management and Budget, Paperwork Reduction Project (0704-0188), Washington, DC 20503.

<b>1. AGENCY USE ONLY (Leave blank)</b>		<b>2. REPORT DATE</b> December 1991	<b>3. REPORT TYPE AND DATES COVERED</b> Technical memorandum	
<b>4. TITLE AND SUBTITLE</b> Trim Drag Reduction Concepts for Horizontal Takeoff Single-Stage-To-Orbit Vehicles			<b>5. FUNDING NUMBERS</b> 505-64-40-01	
<b>6. AUTHOR(S)</b> John D. Shaughnessy and Irene M. Gregory				
<b>7. PERFORMING ORGANIZATION NAME(S) AND ADDRESS(ES)</b> NASA Langley Research Center Hampton, VA 23665-5225			<b>8. PERFORMING ORGANIZATION REPORT NUMBER</b>	
<b>9. SPONSORING / MONITORING AGENCY NAME(S) AND ADDRESS(ES)</b> National Aeronautics and Space Administration Washington, DC 20546-0001			<b>10. SPONSORING / MONITORING AGENCY REPORT NUMBER</b> NASA TM-102687	
<b>11. SUPPLEMENTARY NOTES</b>				
<b>12a. DISTRIBUTION / AVAILABILITY STATEMENT</b>  Unclassified - Unlimited  Subject Category 08			<b>12b. DISTRIBUTION CODE</b>	
<b>13. ABSTRACT (Maximum 200 words)</b> The results of a study to investigate concepts for minimizing trim drag of horizontal takeoff single-stage-to-orbit (SSTO) vehicles are presented. A generic hypersonic airbreathing conical configuration was used as the subject aircraft. The investigation indicates that extreme forward migration of the aerodynamic center as the vehicle accelerates to orbital velocities causes severe aerodynamics instability and trim moments that must be counteracted. Adequate stability can be provided by active control of elevons and rudder, but use of elevons to produce trim moments results in excessive trim drag and fuel consumption. To alleviate this problem two solution concepts are examined. Active control of the center of gravity (c.g.) location to track the aerodynamic center decreases trim moment requirements, reduces elevon deflections, and leads to significant fuel savings. Active control of the direction of the thrust vector produces required trim moments, reduces elevon deflections, and also results in significant fuel savings. It is concluded that the combination of active flight control to provide stabilization, c.g. position control to minimize trim moment requirements, and thrust vectoring to generate required trim moments has the potential to significantly reduce fuel consumption during ascent to orbit of horizontal takeoff SSTO vehicles.				
<b>14. SUBJECT TERMS</b>  Hypersonics, stability and control, trim drag, single-stage-to-orbit			<b>15. NUMBER OF PAGES</b> 31	
			<b>16. PRICE CODE</b> A03	
<b>17. SECURITY CLASSIFICATION OF REPORT</b> unclassified	<b>18. SECURITY CLASSIFICATION OF THIS PAGE</b> unclassified	<b>19. SECURITY CLASSIFICATION OF ABSTRACT</b>		<b>20. LIMITATION OF ABSTRACT</b>